Fachhochschule Aachen(FH)

University of Applied Sciences

Fachbereich Energietechnik

Studiengang Physikingenieurwesen

Thermal behavior of lattice parameter in compounds of the series $Mn_{5-x}Fe_xSi_3$

Bachelorarbeit

von

Ye Cheng

angefertigt am

Jülich Centre for Neutron Science, JCNS-2,

und Peter Grünberg Institut, PGI-4:

Streumethoden

Forschungszentrum Jülich GmbH

September, 2014

Prüfer 1 : Prof. Dr. Arnold Förster

Prüfer 2 : Dr. Karen Friese

Betreuer : Ph.D. Paul Hering

Diese Arbeit ist von mir selbständig angefertigt und verfasst worden. Es sind keine anderen als die angegebenen Quellen und Hilfsmittel verwendet worden.

Ort, den Datum	*Ye Cheng*

Abstract

The magnetocaloric effect (MCE) in paramagnetic materials has been widely used for attaining very low temperatures by applying a magnetic field isothermally and removing it adiabatically. Materials with an increased MCE often show a strong response of the lattice to magnetic phase transitions [1]. In contrast to that this volume effect leads to an increased latent heat and makes the compounds fragile which is disadvantageous for a use in application. Thus thermal evolution of symmetry and lattice parameter needs to be well characterized for candidate materials.

Previous reports [2] predict a hexagonal symmetry for all compounds of the series $Mn_{5-x}Fe_xSi_3$ with x=0, 1, 2, 3, 4 on the basis of complementary X-ray and neutron powder data. Space group P6_3/mcm was found at 293 K. Furthermore magnetic phase transitions at different temperatures in these compounds depending on their iron content [3] have been discovered.

The focus of this analysis is on the thermal behavior of lattice parameter for the compounds Mn_4FeSi_3, $Mn_3Fe_2Si_3$ and $Mn_2Fe_3Si_3$ using X-ray powder diffraction data. Within measurements in the temperature range from 15 K to 300 K all compounds show responses of the lattice to magnetic phase transitions. One, Mn_4FeSi_3, undergoes a structure phase transition from hexagonal to orthorhombic on cooling, which is not reported in the literature.

Contents

4

Chapter 1

Introduction

The magnetocaloric compounds in the system $Mn_{5-x}Fe_xSi_3$ (x=0, 1,..., 5) undergo various magnetic phase transitions at different temperatures depending on their stoichiometry [3]. While the magnetic phase transitions in the system are well characterized, the available information on the temperature dependent behavior of the crystal lattices is limited and needs to be improved. The response of the lattice to the magnetic phase transitions is of special interest because the interplay between the lattice and spin degrees of freedom plays an important role in magnetocaloric materials.

In this thesis, compounds in the series $Mn_{5-x}Fe_xSi_3$ were synthesized by the cold crucible induction melting method. Subsequently, the thermal behaviors of lattice parameters and unit cell volume have been investigated with X-ray powder diffraction measurements in the temperature range from $300\,K$ to $15\,K$. Le Bail refinements [4] were performed with the program Jana2006 [5]. The temperature dependent behavior of the lattice parameter is discussed in relation to the observed magnetic transitions and a comparison of the thermal expansion in the individual compounds with

x=$1, 2, 3, 4$ is presented.

Chapter 2

Background

2.1 The magnetocaloric effect

Magnetocaloric cooling is a promising technology to replace the well-established vapor compression technologies as cooling efficiencies are predicted to be 20 % to 30 % more efficient and the use of hazardous gases can be altogether avoided.

Magnetocaloric cooling technologies are based on the magnetocaloric effect (MCE). This effect describes the change of a temperature of a material under an applied magnetic field. Materials exhibiting a large magnetocaloric effect have a strong coupling between crystallographic structure and magnetic ordering so that a magnetic field can induce a simultaneous change of magnetic and lattice entropies. Thus when the MCE occur, an energy transfer takes place between magnetic moments and lattice degrees of freedom which then leads to a change in temperature of the material.

The refrigeration cycle for a magnetocaloric material with a paramagnetic-ferromagnetic transition consists of the following steps. Starting from a

material in its paramagnetic state ($T > T_c$) an external magnetic field is applied adiabatically. This leads to the ordering of the magnetic moments parallel to the field and a decrease of the magnetic entropy. This decrease is compensated by an increase in the lattice entropy which in turn leads to an increase of the temperature of the material. After this the heat is expelled through an exchange medium and then, the externally applied magnetic field is switched of adiabatically. In the absence of the field the magnetic moments in the material become randomly oriented again. The magnetic entropy increases and therefore the lattice entropy decreases. As a consequence the temperature drops [6]. A scheme of the refrigeration cycle is presented in Figure 2.1.
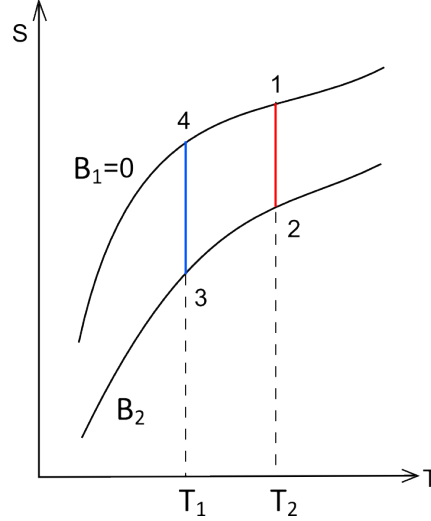
Figure 2.1: Schematic representation of the refrigeration cycle and the involved steps: 1-2: isothermal magnetization (heat release); 2-3: adiabatic demagnetization; 3-4: isothermal demagnetization (heat absorption); 4-1: adiabatic magnetization.

The compounds of the series $Mn_{5-x}Fe_xSi_3$ are promising candidates for magnetocaloric applications as the Curie temperatures for part of the in-

dividual representatives are close to room temperature. In addition, the elements of the material are cheap, abundant and non-toxic. However the major disadvantage of the material is that the magnetocaloric effect is only of moderate size (The largest magnetic-entropy changes in this system are in ferromagnetic $MnFe_4Si_3$ with maximum value of about $4\,J/kg\,K$ for a field chang of $5\,T$ [3].) and further optimization of the materials is required to increase it. This could be done through doping with other elements.

2.2 Current state of research on the compounds in the system $Mn_{5-x}Fe_xSi_3$

The magnetic transitions occurring in the compounds of the system Mn_{5-x}-Fe_xSi_3 have been investigated by magnetization measurements as a function of temperature on powder samples [3]. The temperatures for the magnetic transition are shown in Figure 2.2 for x = 0,..., 5.

For x = 0,..., 3 the paramagnetic phase P transforms to a collinear antiferromagnetic structure AF2. If the temperature is further lowered a second transition to non-collinear antiferromagnetic structure AF1 occurs in all 4 compounds. While the transition temperature P-AF2 increases with increasing x, the temperature for the transition AF2-AF1 decreases with increasing x. With further increase of the Fe concentration (x>3), the magnetic ordering of the compounds is dominated by ferromagnetic interactions and both $MnFe_4Si_3$ and Fe_5Si_3 show only one magnetic transition to a ferromagnetically ordered phase F [3].
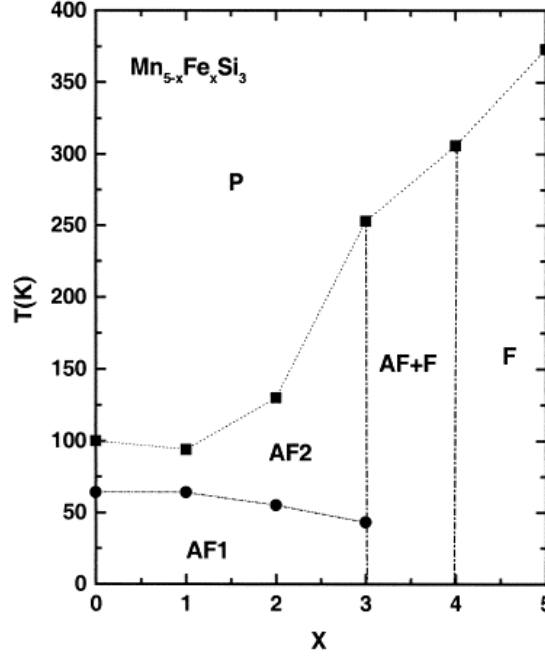
Figure 2.2: Magnetic phase diagram of the $Mn_{5-x}Fe_xSi_3$ system with x=0, 1, 2, 3, 4, 5. Figure from [3].

Previous powder diffraction investigations using X-ray (FeK_α) and neutron sources on the crystal structures [2] have indicated that all the compounds in the system $Mn_{5-x}Fe_xSi_3$ have hexagonal metrics in the investigated temperature ranges. According to these investigations they crystallize in space group $P6_3/mcm$. Each unit cell contains two formula units. The studies were restricted to two temperatures (77 K and 293 K). Table 2.1 shows the published lattice parameter for the compounds of the system at room temperature.

Table 2.1: Lattice parameters of the compounds of the $Mn_{5-x}Fe_xSi_3$ series at room temperature. Data from [2].

| x	$a_0(\mathring{A})$	$c_0(\mathring{A})$	$v_0(\mathring{A}^3)$
0	6.9077±0.00004	4.8131±0.00004	198.90
1	6.8849±0.00009	4.7861±0.00008	196.49
2	6.8538±0.00005	4.7579±0.00005	193.56
3	6.8301±0.00004	4.7390±0.00004	191.46
4	6.8054±0.00007	4.7290±0.00005	189.68

Chapter 3

Theory

3.1 Crystals and crystal systems

A crystal is formed from an ordered arrangement of atoms, molecules, or ions. They are characterized by translation symmetry with the unit cell as the smallest repeat unit. Depending on the shape and symmetry of the unit cell, crystals are classified into seven crystal systems. Their specific conditions, as shown in Table 3.1, affect the lengths (a, b, c) of the unit-cell edges and the angles (α, β, γ) between them.

For the compounds investigated in this thesis two crystal systems, Hexagonal and Orthorhombic, are used to describe the corresponding crystal structures. The hexagonal crystal system has only one Bravais lattice type: simple (P) hexagonal. In the orthorhombic system there are four different Bravais lattices: simple orthorhombic (P), base-centered orthorhombic (C), body-centered orthorhombic (I), and face-centered orthorhombic (F) [7], as presented in Figure 3.1.

Table 3.1: The seven crystal systems, the restrictions on the lattice parameter and the characteristic symmetry elemenst [7].

Crystal System	Axis System	Bravais Lattices	Characteristic Symmetry Element
Triclinic	$a \neq b \neq c$, $\alpha \neq \beta \neq \gamma \neq 90°$	P	Only inversion center possible
Monoclinic	$a \neq b \neq c$, $\alpha = \gamma = 90°$, $\beta \neq 90°$	P, C	Single twofold axis or/and mirror
Orthorhombic	$a \neq b \neq c$, $\alpha = \beta = \gamma = 90°$	P, C, I, F	Three mutually perpendicular twofold axes or/and mirrors
Tetragonal	$a = b \neq c$, $\alpha = \beta = \gamma = 90°$	P, I	One fourfold axis
Rhombohedral	$a = b = c$, $\alpha = \beta = \gamma \neq 90°$	R	One threefold axis
Hexagonal	$a = b \neq c$, $\alpha = \beta = 90°$, $\gamma = 120°$	P, R	One sixfold axis
Cubic	$a = b = c$, $\alpha = \beta = \gamma = 90°$	P, I, F	Four threefold axes

(a)

(b)
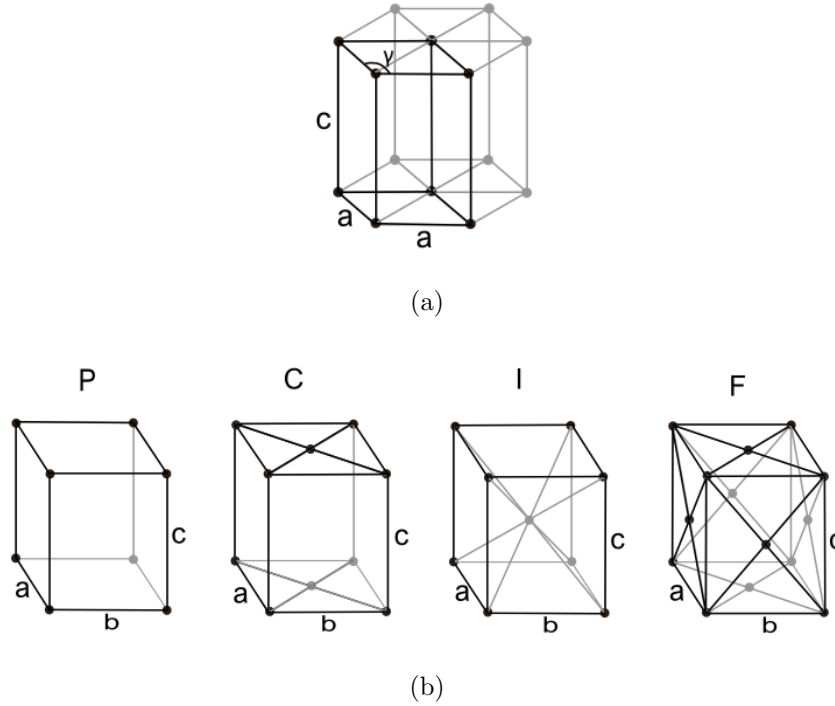
Figure 3.1: Bravais lattices in the (a) Hexagonal and (b) Orthorhombic system.

3.2 Basics of X-ray diffraction

When a focused X-ray beam interacts with atoms in a crystal, a part of the beam is transmitted, a part is absorbed by the sample, a part is refracted and scattered, and a part is diffracted. Diffraction can occur when a beam is scattered by a periodic structure with a repeat distance similar to the wavelength of the beam. Typically, X-rays for a diffraction experiment have wavelengths not exceeding a few angstroms. As this is the typical interatomic distance in crystalline solids, X-rays are a suitable probe for diffraction in crystalline materials.

As mentioned before, a regular three dimensional lattice of points can be considered as the basis of a crystal. From these lattice points, "crystallo-

graphic planes" can be defined on the basis of the position of the atoms
in the crystal. All parallel planes will contain the same arrangement of
atoms. The orientation of the planes in the lattice is defined in terms of
the notation introduced by the English crystallographer William Hallowes
Miller, the "Miller indices", (h k l). Parallel to any plane defined by the
indices (h k l), there exists a family of parallel equidistant planes with a
spacing of d_{hkl} between them. The spacing d is related to lattice constant
a, b and c and it is calculated as follows:

$$\text{for hexagonal crystals:} \quad d_{hkl} = \frac{1}{\sqrt{\frac{4}{3}\left(\frac{h^2+hk+k^2}{a^2}\right) + \left(\frac{l}{c}\right)^2}}$$

$$\text{for orthorhombic crystals:} \quad d_{hkl} = \frac{1}{\sqrt{\left(\frac{h}{a}\right)^2 + \left(\frac{k}{b}\right)^2 + \left(\frac{l}{c}\right)^2}}$$

As shown in Figure 3.2, X-rays are partially scattered by atoms if they
strike the surface of a crystal.
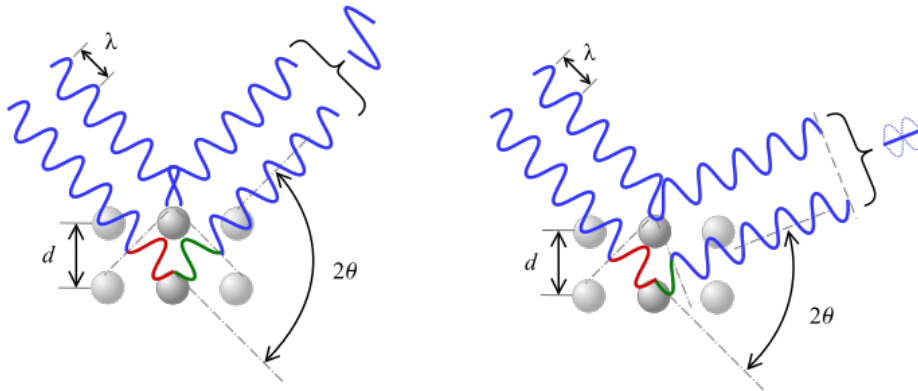
Figure 3.2: Depending on the 2θ angle, the phase shift between different diffracted beams causes
constructive (left figure) or destructive (right figure) interferences. Figure from [8].

The part of the X-ray that is not scattered passes through to the next layer of atoms, where again part of the X-ray is scattered and part passes through to the next layer. If the X-rays diffracted by two different layers are in phase, constructive interference occurs resulting in a reflection in the diffraction pattern. However, if they are out of phase, destructive interference appears and there is no reflection.

The occurrence of constructive interference is explained by Bragg's law (see Figure 3.3):

$$2d_{hkl}\sin\theta = n\lambda$$

If an incoming beam hits a lattice plane under the angle θ, the diffracted beam will also form an angle θ with the lattice planes. The spacing d_{hkl} between two consecutive lattice planes has to correspond to a multiple of the incoming wavelength to get constructive interference of the two scattered waves. Each observed diffraction peak in an X-ray diffraction diagram thus represents a certain lattice plane (h k l).
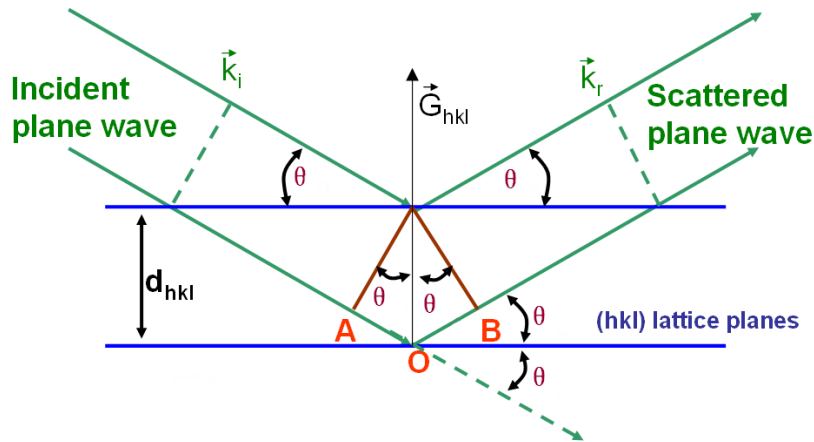

Figure 3.3: Illustration of Bragg's law. Figure from [9].

Since a highly regular structure is needed for diffraction to occur, only crystalline solids will result in sharp diffraction maxima. Amorphous materials will show diffuse diffraction feature which often appear like an increased background in a diffraction pattern.

3.3   X-ray diffraction on polycrystalline samples

A powder sample consists of thousands of crystallites. So a powder can be seen as a polycrystalline material in which all possible orientations of a crystal lattice exist ideally in equal proportions. The lattice planes (h k l) in different crystallites will scatter in different directions and the diffracted beams form a cone. Arcs of the cones are intercepted by a curved strip film surrounding the sample (see Figure 3.4).
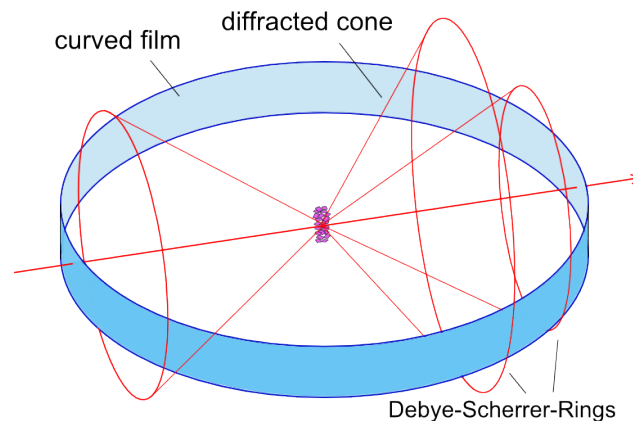

Figure 3.4: X-ray powder diffraction

The higher the point group symmetry of a crystal is, the higher the number of symmetry equivalent lattice planes. Diffraction from symmetry equivalent lattice planes will result in symmetry equivalent reflections (h k l)

with identical θ values that all overlap in the powder diffraction diagram. When two or more diffraction cones from distinct lattice planes have only a small angular difference in 2θ, the diffraction maxima can also overlap, provided the angular difference is smaller than the resolution function of the instrument used for the measurement.

3.4 The Le Bail method

The Le Bail method [4] is a method for the whole pattern decomposition of powder diffraction diagrams. It can be used to determine the space group and unit cell parameter of crystalline compounds. Other parameters which can be fitted simultaneously during a Le Bail refinement include background parameters, the zero shift and parameters describing the shape of the observed peaks.

The Le Bail method is an iterative method: It starts from initial cell parameters, the values of which have to be close to the real values, a diffraction diagram is calculated which is then compared to the observed data. In a least squares procedure the difference between the calculated and observed diagram is then minimized in each point of the diagram by adjusting the lattice parameters, background parameters and parameters of the profile function, which describes the shape of the peaks. With the new parameters a new diffraction diagram is calculated and compared to the observed one. The last steps are repeated till a satisfactory agreement between calculated and observed model is reached. The overall process is shown in Figure 3.5.
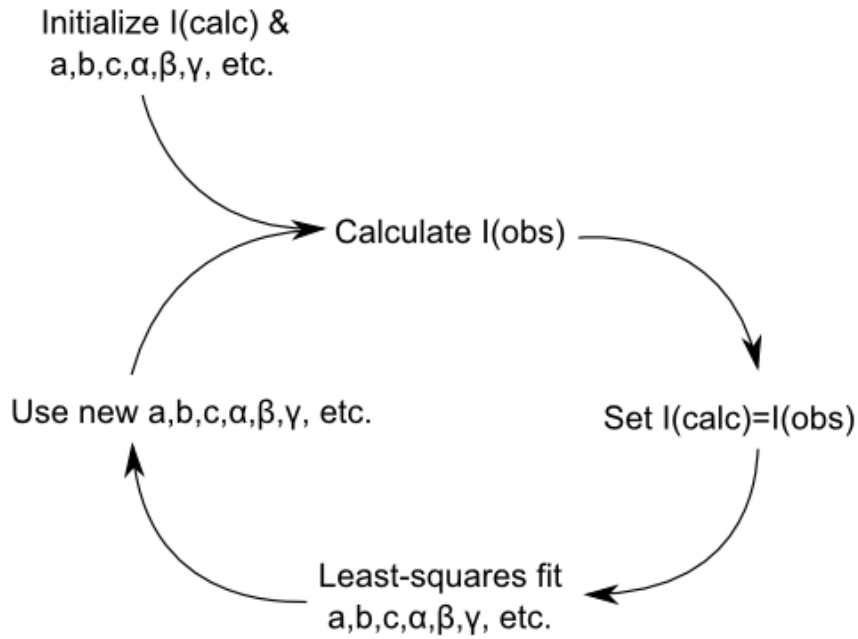
Figure 3.5: Flow chart of Le Bail process. Figure from [10].

In the Le Bail method, standard overall agreement factors, so called R-factors, are used to indicate the quality of the fit to the data. The following two R-factors are generally quoted.

$$\text{Weighted profile R-factor:} \qquad \text{wR}_p = \sqrt{\frac{\sum w(y_{obs} - y_{calc})^2}{\sum wy_{obs}^2}}\%$$

$$\text{Profile R-factor:} \qquad \text{R}_p = \frac{y_{calc} - y_{obs}}{y_{calc}}\%$$

The Le Bail method is an ideal method to follow the change in lattice parameter as a function of temperature. The Le Bail algorithm has been introduced into many programs performing refinement of powder data. In the course of this thesis the program Jana2006 [5] is used for the Le Bail

refinement. Jana2006 is a crystallographic computing system originally developed for incommensurately modulated structures and can be used for the processing of powder and single crystal data.

Chapter 4

Instrumentation

4.1 Cold crucible induction melting

Induction heating is the process of heating a metal by electromagnetic induction, where eddy currents are generated within the metal and resistance leads to joule heating of the metal. The cold crucible combines metal melting and levitation, which requires little or no contact between the material and crucible.

The technique of cold crucible induction melting process [11] is based on the use of a water-cooled structure. The electric field is produced by surrounding the sample with an induction coil through which a high-frequency alternating current (AC) is passed. This allows currents to be generated inside the material contained in the structure. The process is realized in vacuum to ensure a high purity of the resulting material.

A schematic view of the cold crucible setup is shown in Figure 4.1. A water-cooled copper crucible is covered by a glass tube and surrounded with a multi-turn induction coil. The copper crucible is segmented, where

each segment is insulated from each adjacent segment and cooled with water delivered from a water pipe.
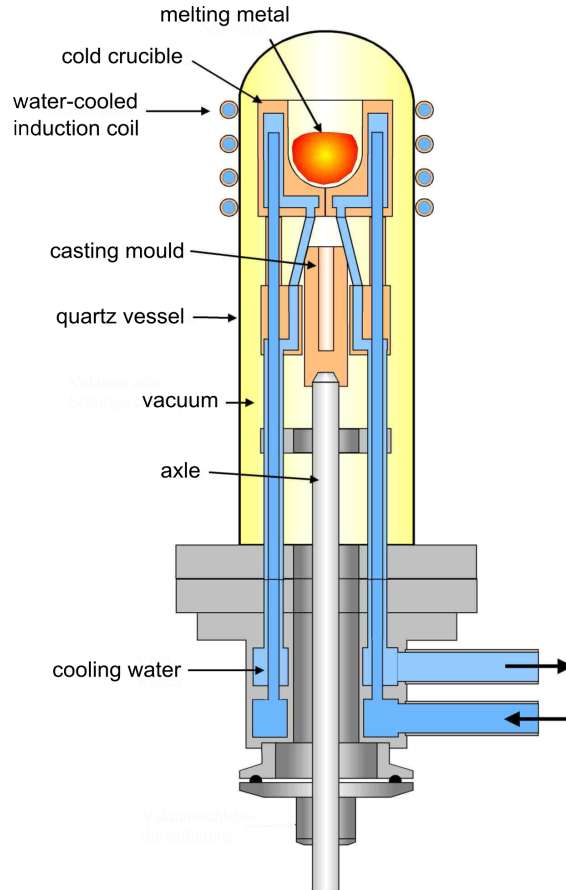
Figure 4.1: Schematic drawing of an apparatus for cold crucible induction melting. Figure from [12].

In a conventional one piece copper crucible the magnetic field is generated by the field current in the heating coil. The magnetic field is cancelled out by the magnetic field associated with the induced current in the crucible. The induced current is looped around each segment as shown by the arrows i_T in Figure 4.2 (a), and allows the generation of an induced current in the metal, creating the required magnetic field in the metallic sample. With an increase in power, the metal is melted by joule heating caused by eddy

currents in a sphere shape.

Once the metal is molten, the charge starts to be partially levitated by the effect of the Lorentz forces which minimizes the thermal losses of the melt and accelerates the process of eventual further heating (see Figure 4.2 (b)). This also prevents any contamination from the released dust as the crucible disintegrates to reach a maximum purity. In addition, the interaction of the induced currents with the magnetic field produce specific Lorentz forces F acting in the melt, which results in their movement in the direction of the dashed arrows. This way, it is possible to carry out constant and well-controlled stirring to provide excellent thermal and chemical homogenization of the melt. Consequently, supplied materials are immediately and successfully melted in a crucible surrounded with the water-cold wall.

(a)   (b)
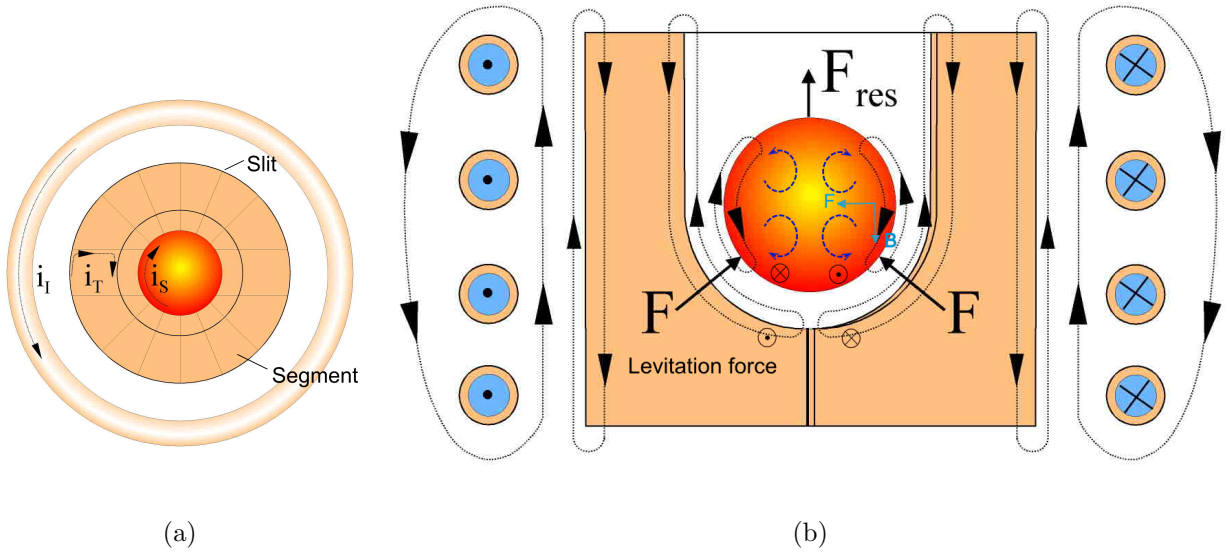
Figure 4.2: Principle of cold crucible induction melting (a) Induced currents (b) Magnetic fields. Figure from [12].

4.2   X-ray powder diffractometer: Huber G670

A coherent scattering pattern on polycrystalline material can be recorded using an X-ray powder diffractometer. In this measurement a Huber Guinier G670 [13] diffractometer was used. The Guinier diffractometer is based on pure K_α-radiation being transmitted through a powder sample and the diffracted beam being recorded on the focusing circle. The basic geometry of the X-ray powder diffractometer used here involves an X-ray tube, a monochromator to choose the correct wavelength, a divergence slit located between the X-ray source and the sample and a X-ray $100°$ area detector situated on the circumference of a graduated circle centered on the powder sample. When a 2-dimensional detector is used to monitor the diffracted radiation, a beam stopper is needed to stop the intense primary beam that has not been diffracted by the sample to avoid damage of the detector. Figure 4.3 shows a schematic drawing of the setup.
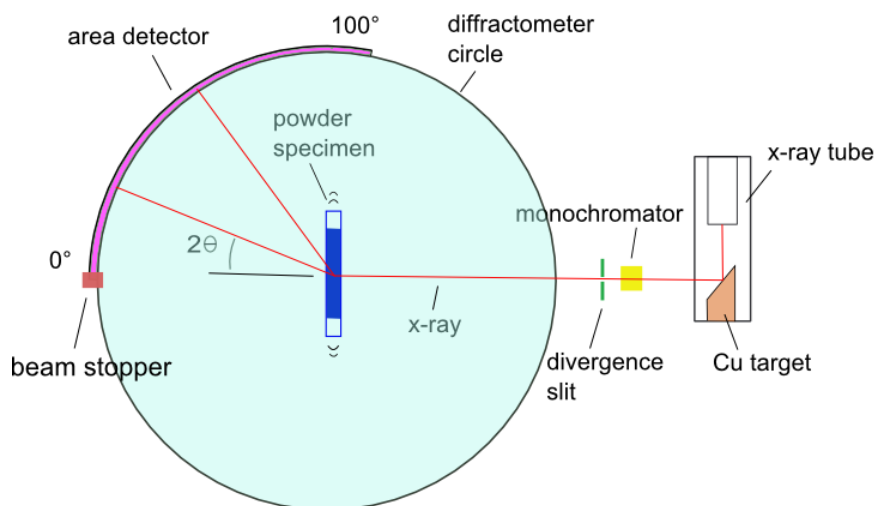
Figure 4.3: Schematic of X-ray diffractometer

X-rays are generated in a cathode ray tube by heating a filament to produce electrons, accelerating the electrons toward a target Cu by applying a voltage, and bombarding the Cu with electrons. Provided the electrons have sufficient energy to dislodge inner shell electrons of the target material, characteristic X-ray spectra are produced when the excited electrons fall back to their original state. By placing a suitable monochromator and a divergence slit between the X-ray tube and the sample, it is possible to select exclusively only the CuK_α-radiation, which is then directed to the sample. As the CuK_α-radiationis diffracted at a slightly different angle, it is possible to direct it away from the sample. The CuK_α-radiation enters the sample with an angle of incidence of $45°$ while the sample moves asymptotically to the focal circle and back to bring as many grains as possible into diffraction condition.

An imaging plate with a 2θ range from $0°$ to $100°$ with the step size of $0.005°$ is used as 2-dimensional detector. The image plate foil is positioned in the Guinier camera 670 on the focal circle. A complete diffractogram for the $100°$-detector thus consists of 20,000 data points with a step resolution of $0.005°$. Apart from the imaging plate, a laser recording unit with a photomultiplier and preamplifier and a halogen lamp are also located inside the housing of the 670 camera. After the imaging plate is exposed by the X-rays, the image plate is scanned with the laser unit by a vertical beam within approx. 5 seconds. During the scanning process, the blue photo stimulated luminescence is excited from the areas which have been subjected to X-ray exposure. Afterwards the blue photo stimulated luminescence is amplified by the photomultiplier tube and registered. The

halogen lamp is then used to delete the information recorded on the imaging plate. After this process the Guinier camera is ready for recording the next image.

The obtained signal will be amplified and digitized by an A/D-converter and transferred to the memory of the controlling computer. Thus it is capable of providing digital powder diffractograms within relatively short time which can then be processed further by software analysis. The data is usually presented as the scattered intensity versus the diffraction angle.

Chapter 5

Experimental procedures

5.1 Synthesis of the powder samples

The polycrystalline sample of Mn_4FeSi_3 was prepared by heating stoichiometric amounts of the pure $(3\,N)$ elements Mn, Fe and Si, which were weighed based on the respective mass ratios of the compounds, with the method of cold crucible induction melting [13].

First of all, pieces of Mn, Fe and Si were put into the copper crucible with tweezers. To prevent the small metal pieces from falling into the slit, the larger metal pieces were put at the bottom. During the following process the crucible was covered hermetically with a glass tube. In order to remove the oxygen the sample chamber was pumped under vacuum before melting the materials.

To remove impurities from the surface the sample was carefully heated under vacuum until it started to glow and till the pressure in the sample chamber stabilized. After this step the chamber was filled with argon and the melting process was started in a high purity argon atmosphere. Figure

5.1 shows a photo of the cold crucible setup in operation. The resulting ingot after cooling down was turned upside down and melted and cooled three additional times to ensure thermal and chemical homogenization of the melt.
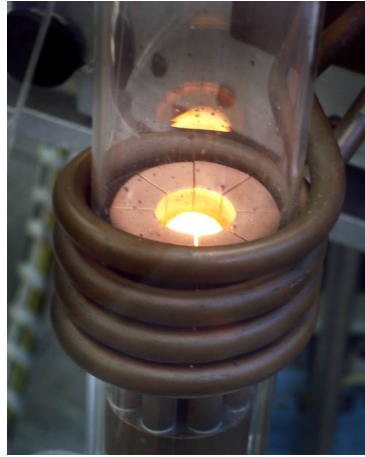
Figure 5.1: Photo of the melting process of the material in the cold crucible induction melting.

Two other samples, $Mn_3Fe_2Si_3$ and $Mn_2Fe_3Si_3$, were prepared in the same way. The completion of the three samples needed several hours. The weight loss after the final melting was less than 0.5% for all three samples.

5.2   X-ray powder diffraction experiments

For X-ray powder diffraction the grain size of the powder should be in the range of 1 to 50 microns, as, if the crystallites in the sample are very large, there will not be a smooth distribution of crystal orientations which leads to a preferred orientation effects in the powder diffraction diagram. The synthesised ingots of the materials were crushed and grinded by hand until

a homogenous powder with a grain size of 20 to 30 microns was obtained. In order to fix the powder to the sampler holder, cellophane foil was used. Since the foil is amorphous and does not have a long range order periodicity, its contribution to the powder diffraction diagram is only seen as a slight increase of the background in the lower θ-angles.

To prepare the sample on the foil the following procedure was used: first about 1 mg powder was put in the middle of a small, rectangular thin film, than ethanol was dripped onto the powder to ensure that the layer of powder has a uniform thickness. After the powder dried totally, it was covered with another foil. Finally these two foils were fixed together with a metal ring. Then the powder sample could be attached to the sample holder.

The sample holder was placed in the Huber G670 camera which operates in transmission mode. With a wavelength of monchromatic CuK_{α}- radiation (λ=1.54 Å) the Bragg angle from 0° to 100° with the step size of 0.005° in 2θ was recorded on the imaging plate. The total exposure time was 120 minutes.

For the low temperature measurements the Huber G670 diffratometer was combined with a closed cycle He cryostat. Powder diffraction diagrams were recorded every 5 K in the temperature range from 300 K to 15 K. It thus took about 3 days to complete the whole powder diffraction measurements on one sample in the full temperature range.

5.3   Le Bail refinements of the powder diffraction data

After data acquisition with the powder diffractometer for $Mn_{5-x}Fe_xSi_3$
compounds, the data processing was started with Jana2006 [5], using the
Le Bail method [4].

For the Le Bail method, the unit cell and the approximate space group of
the sample must be predetermined to have a good starting model for the
fitting procedure. From the literature it is known that the $Mn_{5-x}Fe_xSi_3$
compounds crystallize in the space group $P6_3/mcm$ at room temperature
and that the lattice parameters are $a = b \approx 6.88\,\text{Å}$ and $c \approx 4.79\,\text{Å}$. After
reading in the data files in Jana2006 a manual background was created
for each of them and the first $27°$ of the powder diffraction diagrams were
excluded as the background shape was irregular and difficult to fit in this
region. First the lattice parameter a, b and c, and the zero shift were
refined. The observed peak shapes were modeled using the pseudo Voigt
function which is a convolution of Gaussian profile (parameter GW) and
Lorentzian profile (parameter LY) functions. In order to get a proper error,
Berar's correction [14] was applied. The refinement is an iterative process
and normally 10 to 100 times cycles are required. Refinement was stopped
when the change in the all parameters was less than $1\,\%$. The Le Bail re-
finement was repeated for all patterns in the temperature range of $15\,\text{K}$ to
$300\,\text{K}$. At each of the temperatures the parameters from the next highest
temperature point were used as starting values. Typical final agreement
factors R_p lie in the range of $0.85\,\%$ to $1.10\,\%$ and the overall fit of the data
is excellent.

During the analysis of the diffraction patterns of Mn_4FeSi_3, it became evi-

dent that a satisfactory fit of the data at the lowest temperature was not possible assuming hexagonal metrics. The overall agreement factor for this compound at $15\,K$ was R_p $1.46\,\%$. Though this indicates a good fit, it is still approximately $0.5\,\%$ worse than the fits achieved at higher temperatures. The low temperature data of this compound were therefore fitted assuming orthorhombic space group symmetry Cmcm, which is a maximal subgroup of the hexagonal space group $P6_3/mcm$ (see section 3.1). With the reduced symmetry the R_p value dropped to $0.94\,\%$. The orthorhombic space group was used for all temperature between $65\,K$ and $15\,K$ for Mn_4FeSi_3 and leads to an excellent agreement between observed and calculated diffraction diagram.

For the other two compounds, $Mn_3Fe_2Si_3$ and $Mn_2Fe_3Si_3$, space group $P6_3/mcm$ leads to excellent fits of the data in the whole temperature range and a reduction of the symmetry was not necessary.

Chapter 6

Results and discussion

6.1 Analysis of X-ray powder diffraction data of Mn$_4$FeSi$_3$ (x=1)

As mentioned before, according to the literature all compounds from the system Mn$_{5-x}$Fe$_x$Si$_3$ crystallize in a hexagonal structure with space group P6$_3$/mcm [2]. This was deduced from earlier powder diffraction studies on the compounds which were, however, restricted to measurements at two temperatures (77 K and 293 K).

Our powder diffraction experiments on Mn$_4$FeSi$_3$ were performed in the temperature range from 300 K to 15 K with steps of 5 K. The Le Bail refinement [4] of the data in the temperature range from 75 K to 300 K is consistent with the hexagonal space group P6$_3$/mcm. Figure 6.1 shows the final refinement for the data at 75 K and, as can be seen, the differences between the observed and the calculated diffraction diagram are very small. This is reflected in excellent agreement factors of R$_p$=1.09 %.
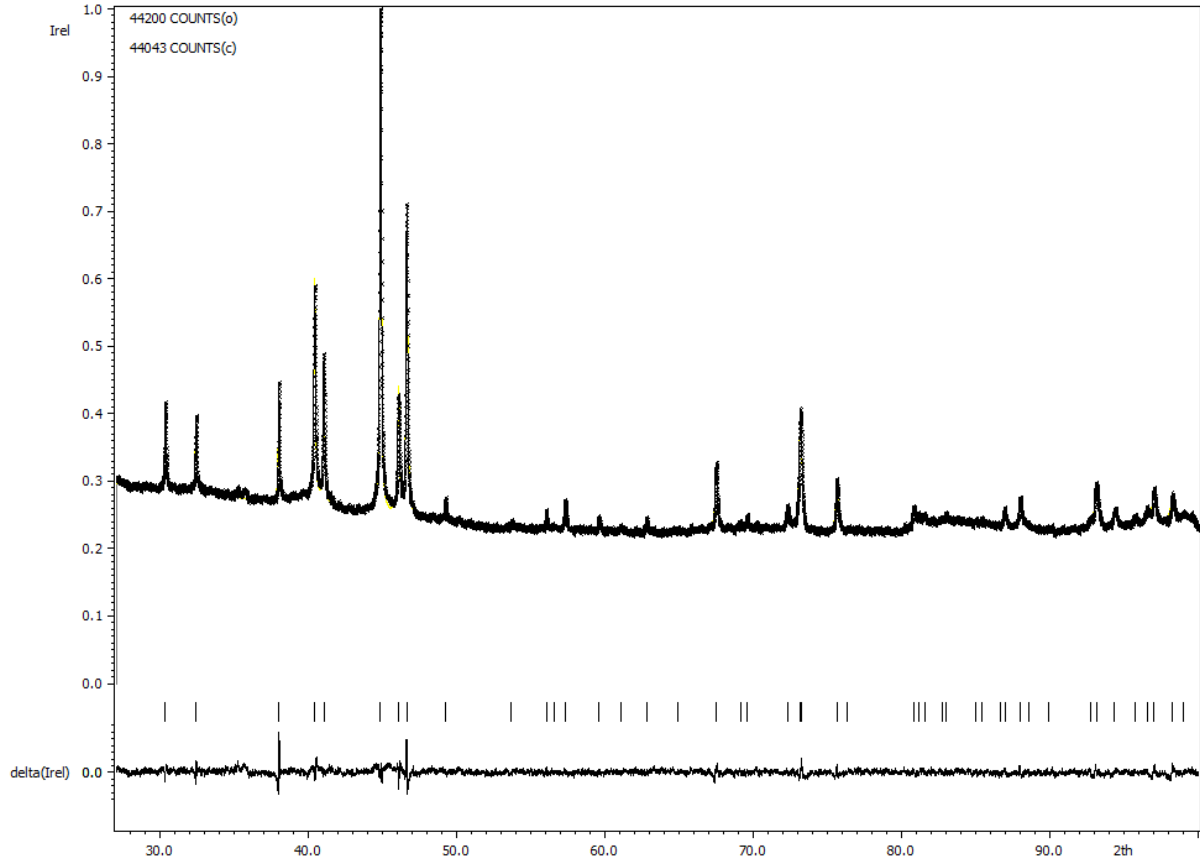
Figure 6.1: Observed, calculated and difference profile for Mn_4FeSi_3 at 75 K from the Le Bail refinement [4] using the $P6_3/mcm$ space groups. The calculated positions of the reflections are given by the vertical bars. Refinement was performed with the program Jana2006 [5].

However, at temperatures lower than 75 K, a part of the peaks get significantly broadened and with a further decrease of the temperature a clear splitting is observed. This observation suggests that a structural transition takes place in Mn_4FeSi_3 in the vicinity of a temperature of 75 K.

The changes in the diffraction diagram suggest that the compound undergoes a phase transition to a crystal structure which crystallizes in a

subgroup of P6$_3$/mcm. From all the maximal subgroups of P6$_3$/mcm only one does not maintain the trigonal (or hexagonal) metrics and would thus lead to a splitting of peaks in the diffraction diagram. This is the orthorhombic space groups Cmcm. The relationship between the hexagonal cell and the orthorhombic C-centered cell is illustrated in Figure 6.2. The hexagonal cell can be transformed to an orthohexagonal setting using the transformations a$_{ortho}$=2 a$_{hex}$+b$_{hex}$, b$_{ortho}$=b$_{hex}$, c$_{ortho}$=c$_{hex}$. For the undistorted orthohexagonal cell this implies an a$_{ortho}$/b$_{ortho}$ ratio of $\sqrt{3}$.
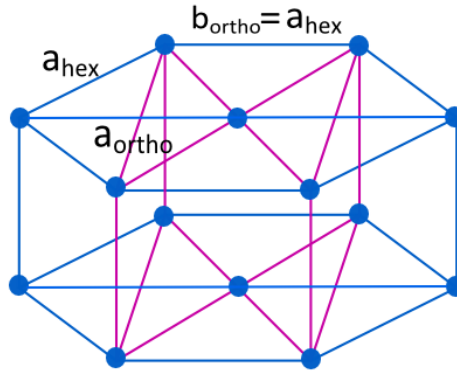

Figure 6.2: Illustration of the transformation from the hexagonal to the orthohexagonal cell.

Assuming orthorhombic Cmcm space group for the low temperature polymorph (70 K - 15 K) of Mn$_4$FeSi$_3$ a Le Bail refinement was performed. As can be seen from Figure 6.3, the Le Bail refinement of the data assuming the orthorhombic space group leads to a significantly better fit than the hexagonal model and the splitting of reflections is very well reproduced assuming the lower symmetry.
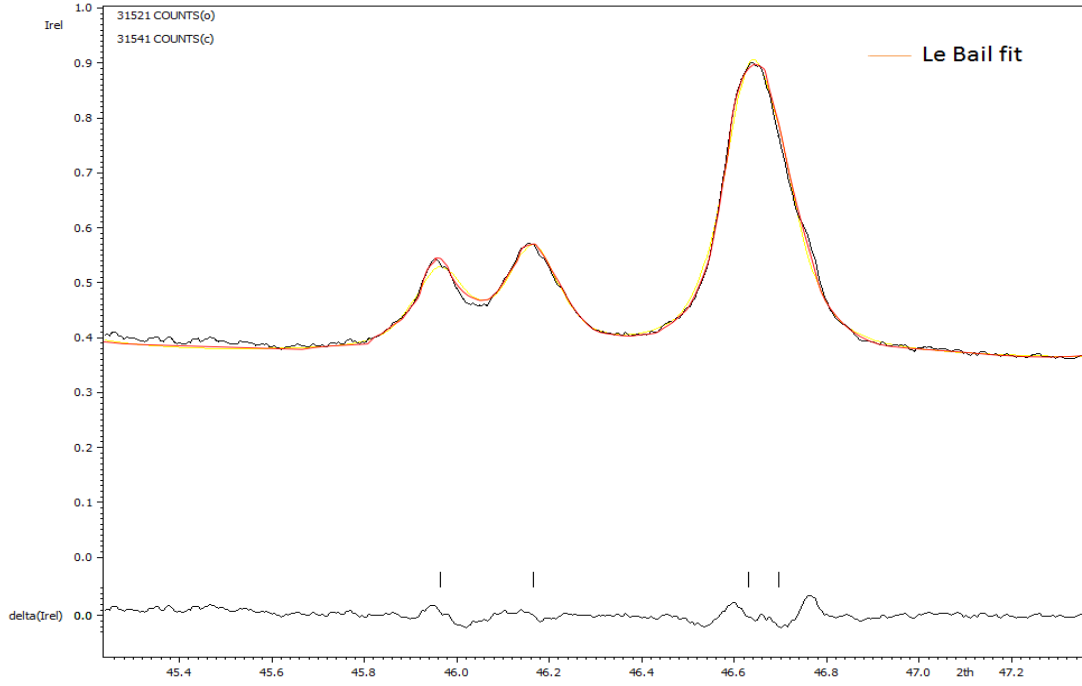
(a)
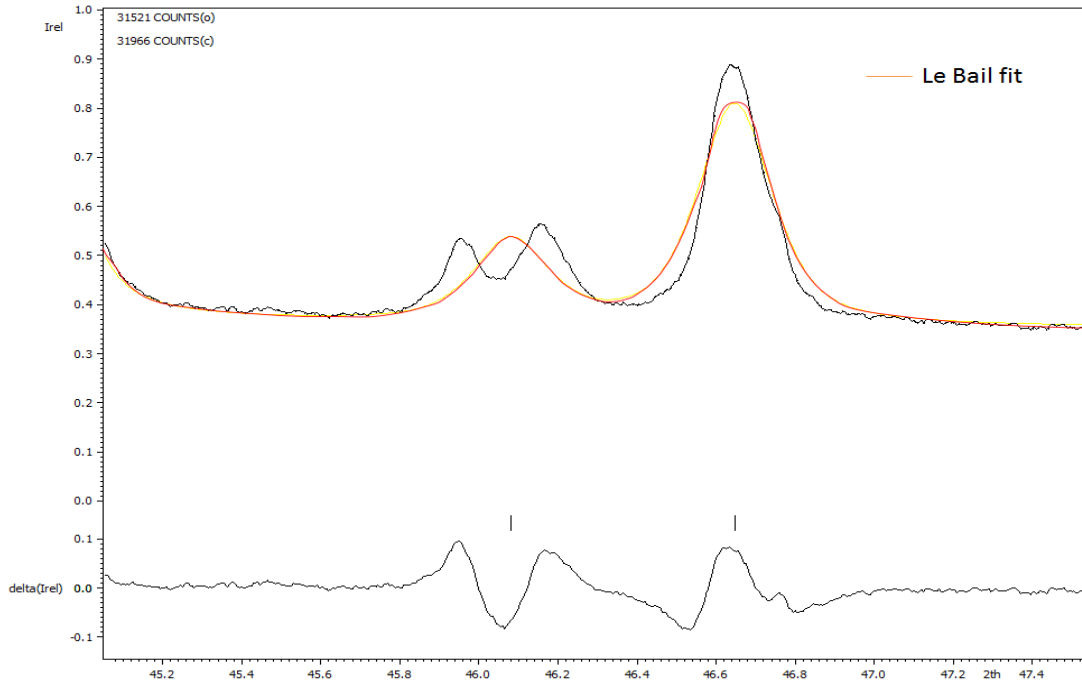
(b)

Figure 6.3: Detail of the observed, calculated and difference profiles for the Le Bail fit of Mn_4FeSi_3 at 15 K in (a) space group Cmcm (R_p=0.94 %) and (b) in space group $P6_3$/mcm (R_p=1.46 %).

In order to obtain the phase transition temperature, in which the hexagonal structure transforms into the orthorhombic structure, the a/b ratio was calculated using the cell parameters obtained from the Le Bail fits (Table 6.1).

Between 60 K and 65 K the a/b ratio approaches $\sqrt{3}$, which means that at temperatures higher than 65 K the structure can be described in the higher symmetry of P6$_3$/mcm. Thus the exact transition temperature has to in the range between 60 K and 65 K.

Table 6.1: Lattice parameter and a/b ratio for the refinements of Mn$_4$FeSi$_3$ in space group Cmcm.

T (K)	a (Å)	b (Å)	c (Å)	a/b
15	11.9134	6.84013	4.76844	1.74169204
20	11.91391	6.84049	4.76843	1.74167494
25	11.91282	6.84074	4.76892	1.74145195
30	11.91098	6.84001	4.76774	1.7413688
35	11.91108	6.84202	4.76825	1.74087185
40	11.90873	6.84264	4.76801	1.74037068
45	11.90585	6.84333	4.76772	1.73977435
50	11.90284	6.84496	4.76752	1.73892032
55	11.89812	6.84517	4.76834	1.73817743
60	11.89318	6.8457	4.76749	1.73732124
65	11.87085	6.86562	4.76751	1.72902811
70	11.87241	6.86375	4.76719	1.72972646

Figure 6.4 pictures the thermal evolution of the unit cell of Mn$_4$FeSi$_3$. In comparison to a hexagon of three combined hexagonal unit cells of the compound at 300 K. At the top left of the figure the thermal contraction

of the hexagonal unit cell from $300\,\text{K}$ to $65\,\text{K}$ is illustrated. The top tight part of the figure illustrates the change when the structural transition is passed and the symmetry is changed to orthorhombic. In the orthorhombic phase the a and b lattice parameter develop independently. The lower part of the figure illustrates the overall change of the lattice at the different temperatures in a projection along the c-axis.


(a)

(b)

(c)

—— 300 K (hexagonal)

—— contraction from 300K to 65K (hexagonal)

—— 15 K (orthorhombic)
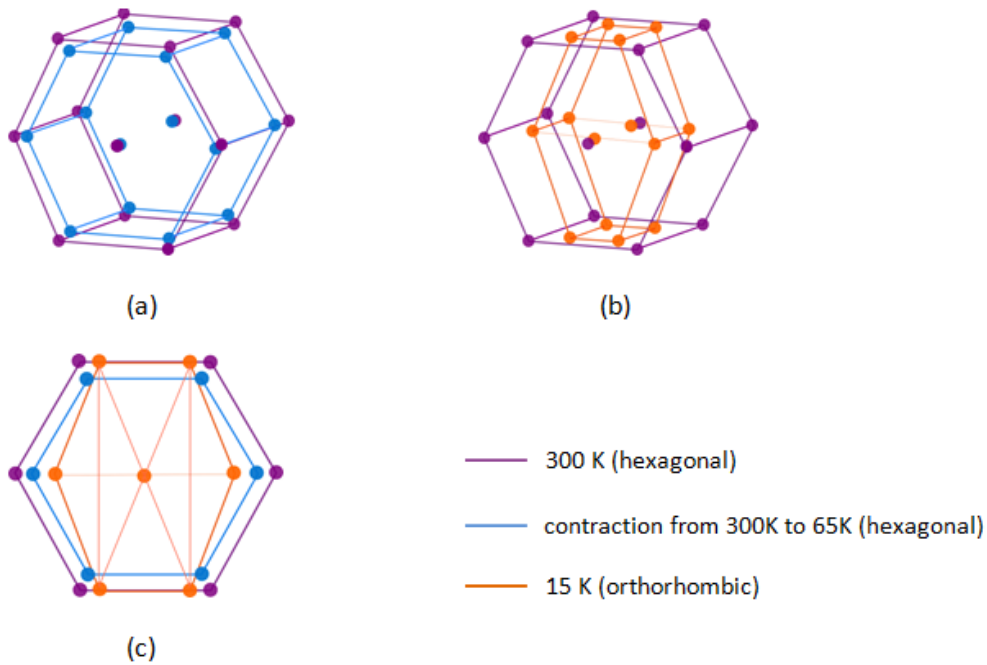
Figure 6.4: Illustration of the changes of the unit cell in Mn_4FeSi_3 on cooling

In order to examine the changes in the structure of Mn_4FeSi_3 in detail, the volumes of the unit cell for all temperature steps were calculated. The a_{ortho}-lattice parameter and the unit cell volume in the orthorhombic phase were divided by $\sqrt{3}$ to make it comparable to the hexagonal parameter. The lattice parameter and unit cell volume at $300\,\text{K}$ were taken as reference

and the relative values of all lattice parameters and unit cell volumes in the temperature range of 15 K to 300 K were obtained by normalizing with the values from 300 K. The diagram of the relative values of the lattice parameters and unit cell volumes versus temperature is presented in Figure 6.5 (a). One can clearly see the phase transition reflected in the lattice parameter.

In the temperature range from 300 K to 65 K both a$_{hex}$ (b$_{hex}$)- and c$_{hex}$-lattice parameter decrease smoothly and in a comparable degree. The unit cell volume also decreases smoothly in this temperature range. With a zoom on the parameters at temperature around 94 K (Figure 6.5 (b)), one can see a bump in c$_{hex}$-lattice parameter and also a valley in the a$_{hex}$ (b$_{hex}$) -lattice parameter at 80 K.

At the phase transition $\sqrt{3} \cdot$ a$_{ortho}$ starts to increase while at the same time b$_{ortho}$ decreases. The c$_{ortho}$ lattice parameter shows a very small increase in the temperature range from 60 K to 15 K. The unit cell volume also slightly increases in this temperature range. The divergence of the unit cell volume from the smooth trend close to the phase transition temperature is probably related to the rather large step size of 5 K. Measurements using a finer step size (which are out of the scope of this work) would be necessary to investigate this further.
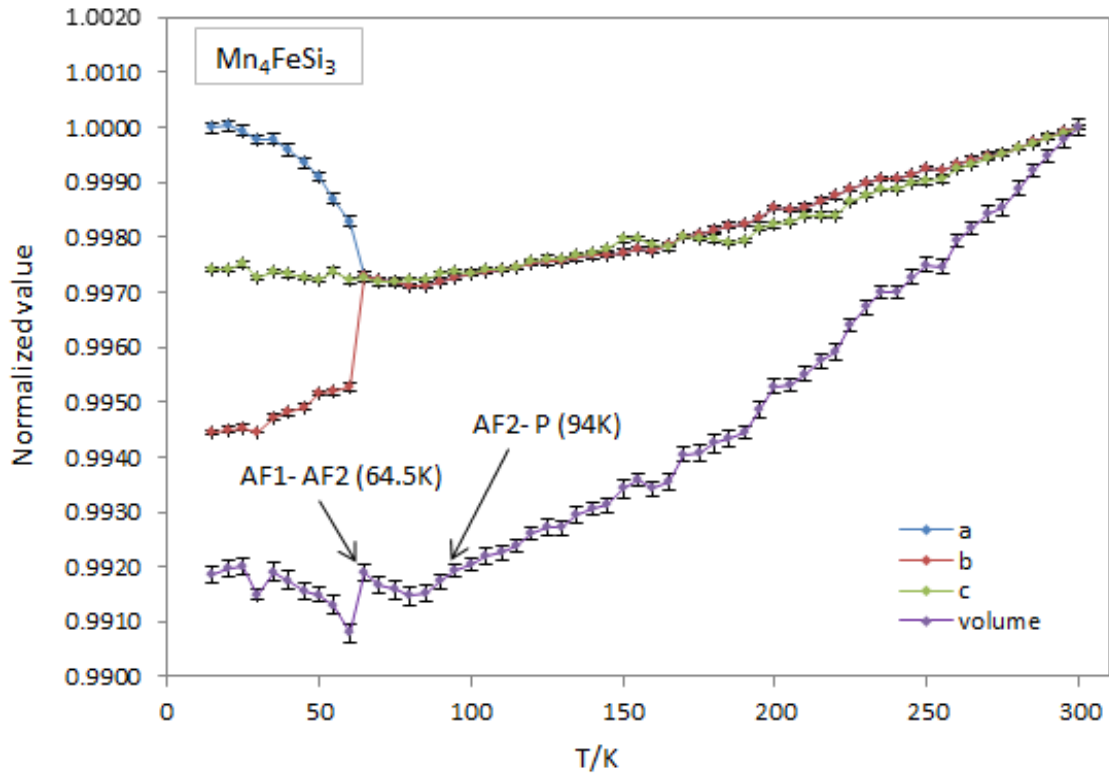
(a)
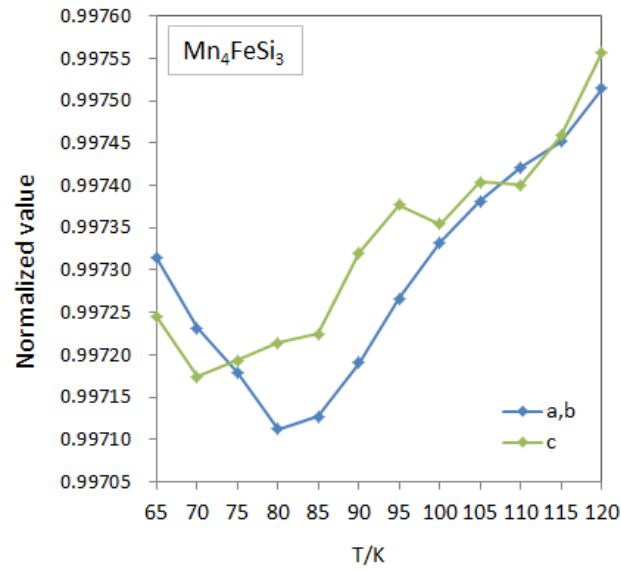
(b)

Figure 6.5: Normalized values of lattice parameters and unit cell volume of Mn_4FeSi_3 versus temperature. The a-lattice parameter and the unit cell volume in the orthorhombic phase were divided by $\sqrt{3}$ to keep the data comparable to the hexagonal parameters. Temperatures of the transition to magnetically ordered phases are indicated.

As mentioned in section 2.2, it is known that all compounds in the series Mn$_{5-x}$Fe$_x$Si$_3$ have one or more transitions to magnetically ordered phases as a function of temperature. For Mn$_4$FeSi$_3$ (x=1) two magnetic transitions have been found [3]: at 94 K the paramagnetic state transforms to a collinear antiferromagnetically ordered AF2 state which reflected in c$_{hex}$-lattice parameter. At 64.5 K a second transition from the collinear antiferromagnetic state to a non-collinear antiferromagnetic phase AF1 is observed.

The temperature of the AF2 to AF1 transition nearly coincides with the structural transition from hexagonal to orthorhombic. Further investigation is needed to investigate the interplay between magnetic and structural transition in this temperature range. As can be seen the transition from the paramagnetic to the collinear antiferromagnetic AF2 phase is also visible in the lattice parameter, in particular by a slight change of trend for the c-lattice parameter.

6.2 Analysis of X-ray powder diffraction data of Mn$_3$Fe$_2$Si$_3$ (x=2)

The data analysis of Mn$_3$Fe$_2$Si$_3$ was performed analogous to the one of Mn$_4$FeSi$_3$ using the Le Bail refinement algorithm [4] implemented in Jana2006 [5]. In this case the symmetry P6$_3$/mcm was used for the whole temperature range (300 K - 15 K) as there is no broadening or splitting of reflections observable at any of the temperatures. The fit of the data led to excellent agreement factors with R$_p$ values in the range of 1.09 % to 1.26 %.

The temperature dependence of the normalized lattice parameters and unit cell volumes are shown in Figure 6.6. As can be seen, all three lattice parameter and the unit cell volume decrease smoothly with only small variations as a function of temperature.
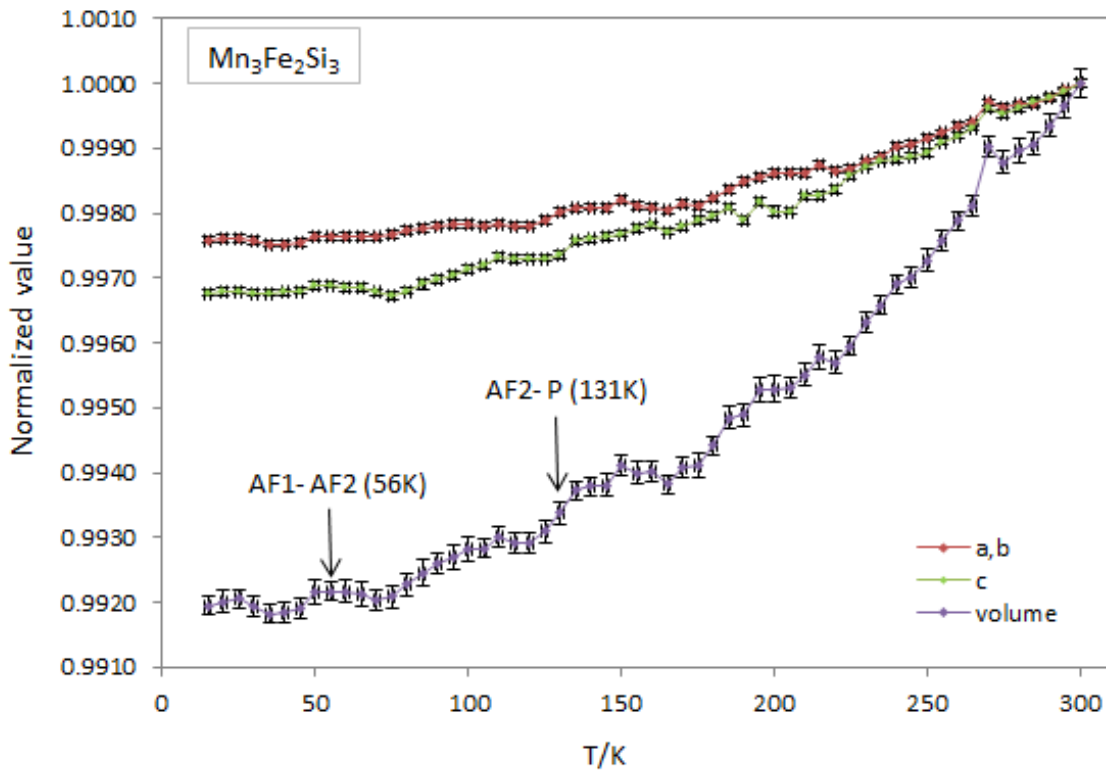
Figure 6.6: Normalized values of the lattice parameter and unit cell volume of $Mn_3Fe_2Si_3$ versus temperature. Temperatures of the transition to magnetically ordered phases are indicated.

In contrast to Mn_4FeSi_3 where a and c lattice parameter of the hexagonal phase show a nearly identical relative decrease with temperature, in $Mn_3Fe_2Si_3$ the value of the c-lattice parameter is significantly more reduced than the value of the a (b)-lattice parameter. Like Mn_4FeSi_3, $Mn_3Fe_2Si_3$ also has magnetic phase transitions at $56\,K$ and $131\,K$ [3], respectively.

As can be seen from Figure 6.6, there is no clear sign of a response of the lattice to the two magnetic transitions. At a temperature of about 270 K a small anomaly for the a (b)- and c-lattice parameter and the unit cell volume is observed. This might be ascribed to erroneous data points, however, earlier investigations on Mn$_4$FeSi$_3$ (see Figure 6.7 (b)) with the same diffractometer have shown that the lattice parameter resulting from measurements on this instrument are in excellent agreement with lattice parameter obtained from neutron powder data measured on the high resolution diffractometer SPODI at the MLZ in Garching, Germany. This can be seen as a proof that the data measured on the Huber diffractometer are very reliable and the observed anomaly in Mn$_3$Fe$_2$Si$_3$ is therefore likely to be real. Further investigations are therefore warranted.

6.3 Analysis of X-ray powder diffraction data of Mn$_2$Fe$_3$Si$_3$ (x=3)

Like for the other compounds, the data sets corresponding to Mn$_2$Fe$_3$Si$_3$ in the temperature range from 300 K to 15 K (step size 5 K) were also refined using the Le Bail method [4] with the program Jana2006 [5]. Again the space group P6$_3$/mcm was used for the whole temperature range, as no indications of a symmetry change have been observed. The resulting overall agreement factors indicate an excellent fit at all temperatures (R$_p$ in the range from 0.79 % to 0.85 %).

The normalized temperature dependent lattice parameter and unit cell volume are plotted in Figure 6.7 (a). They show an unusual thermal expansion

of the lattice parameter. If one disregards the small anomaly at 35 K, the c-lattice parameter follows the expected behavior and continuously decreases as a function of temperature. The a (b)-lattice parameter, on the other hand, decrease in the temperature range from 300 K to 180 K and start to continuously increase down to 15 K. The fluctuation of a-, c-lattice parameters and the unit cell volume at approximately 255 K coincides with the temperature of the magnetic transition at 254 K observed by other authors [3]. However, the negative thermal expansion of the a (b)-lattice parameter in the low temperature range is not directly related to any magnetic transition. At approximately 35 K a small anomalous increase is observed in the lattice parameter and unit cell volume, which might be triggered by the magnetic transition at 42 K observed in [3]. Though this might be related to an outlying data point, it is interesting to note that a similar anomaly was observed earlier in $MnFe_4Si_3$ [15] at 15 K based on X-ray and neutron powder data (Figure 6.7 (b)). This anomaly would therefore require further investigation with a smaller temperature step which is, however, out of the scope of this study.
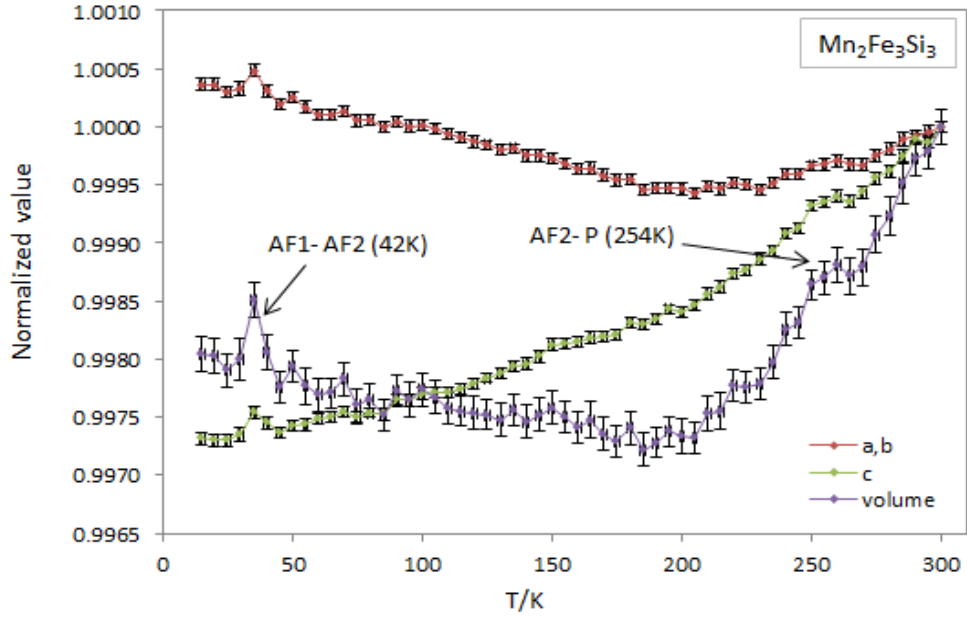
(a)
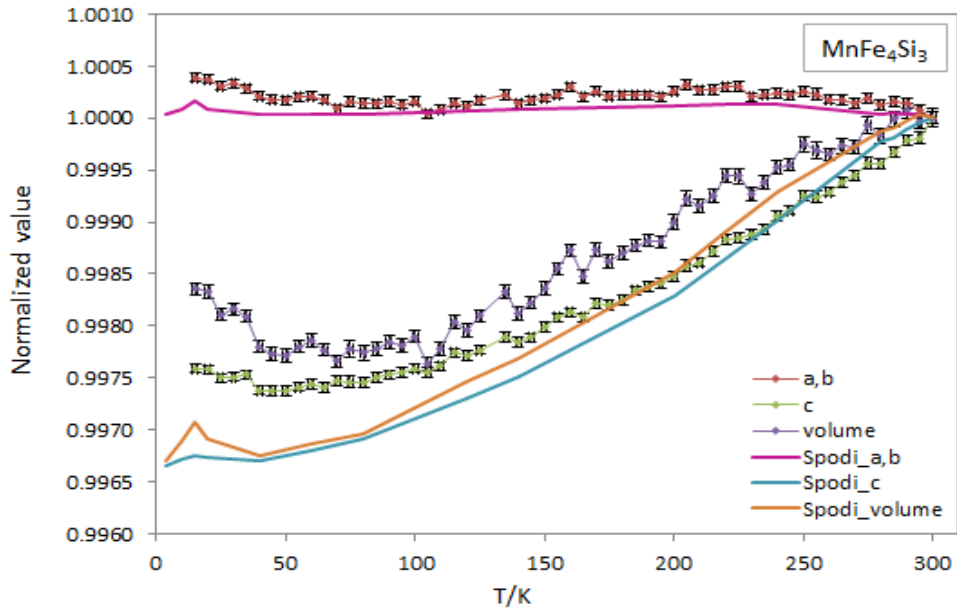
(b)

Figure 6.7: Normalized values of the lattice parameter and unit cell volume of $Mn_2Fe_3Si_3$ and $MnFe_4Si_3$ versus temperature. Temperatures of the transition to/between magnetically ordered phases for $Mn_2Fe_3Si_3$ are indicated. For $MnFe_4Si_3$ lattice parameters resulting from X-ray and neutron powder diffraction experiments are indicated. Neutron data for $MnFe_4Si_3$ were measured on the high resolution powder diffractometer SPODI at MLZ in Garching, Germany. Data for $MnFe_4Si_3$ have been taken from [15].

6.4   Comparison of the room temperature lattice parameter to the values from literature

A comparison of the obtained lattice parameter for $Mn_{5-x}Fe_xSi_3$ (x=1, 2, 3) is given in Table 6.2. As can be seen all the lattice parameter obtained in this work are systematically smaller than the ones published earlier by [2]. However, the resulting c/a ratios are comparable indicating that although there is an offset in the absolute values of the lattice parameter, the relationship of a- and c-lattice parameter are identical within error.

Table 6.2: The room temperature lattice parameter obtained in this work compared to the data from the literature [2]. All standard deviations are given without applying Berar's correction [14].

| x	a, b (Å)		c (Å)		c/a	
	Data from [2]	This work	Data from [2]	This work	Data	This work
1	6.8849 ± 0.00009	6.87786 ± 0.00006	4.7861 ± 0.00008	4.78028 ± 0.00004	0.69515	0.69502
2	6.85385 ± 0.00005	6.8532 ± 0.0001	4.75795 ± 0.00005	4.75603 ± 0.00007	0.69420	0.69399
3	6.83014 ± 0.00004	6.82009 ± 0.00009	4.73904 ± 0.00004	4.73386 ± 0.00006	0.69384	0.69411

6.5   Comparison of the temperature dependent behavior of the $Mn_{5-x}Fe_xSi_3$ compounds (x=1, 2, 3, 4)

A comparison of the thermal behavior of the lattice parameter and unit cell volume for the individual compounds in the series $Mn_{5-x}Fe_xSi_3$ is shown in Figure 6.8. In general, with an increasing iron content the size of the

unit cell decreases. This is easily understandable if one takes into account that the atomic radius of iron (r(Fe)=156 pm) is smaller than the one of Manganese (r(Mn)=161 pm).

As one can see in Figure 6.8 the a (b)-lattice parameter in the four hexagonal phases behaves significantly different. For Mn_4FeSi_3 in the hexagonal phase the largest relative decrease is observed down to the transition temperature. The $\sqrt{3}$a- and b-lattice parameters in the orthorhombic phase exhibit a comparatively drastic change in the low temperature region from 65 K to 15 K. For $Mn_3Fe_2Si_3$ the a (b)-lattice parameter also decreases smoothly in the higher temperature region, yet the slope is reduced towards lower temperatures. For $Mn_2Fe_3Si_3$ only a small decrease of the a (b)-lattice parameter is observed in the high temperature region followed by a clear negative thermal expansion in the low temperature region. In $MnFe_4Si_3$ the relative changes of the a (b)-lattice parameter are the smallest and altogether there is a slight increase of the a (b)-lattice parameter over the whole temperature range.

The c-lattice parameter has a far more uniform behavior and the curves in all four compounds have almost the same slope. Finally, the behavior of the unit cell volume in the four compounds basically reflects the changes of the a-lattice parameter and changes the most for the compounds Mn_4FeSi_3 and $Mn_3Fe_2Si_3$.
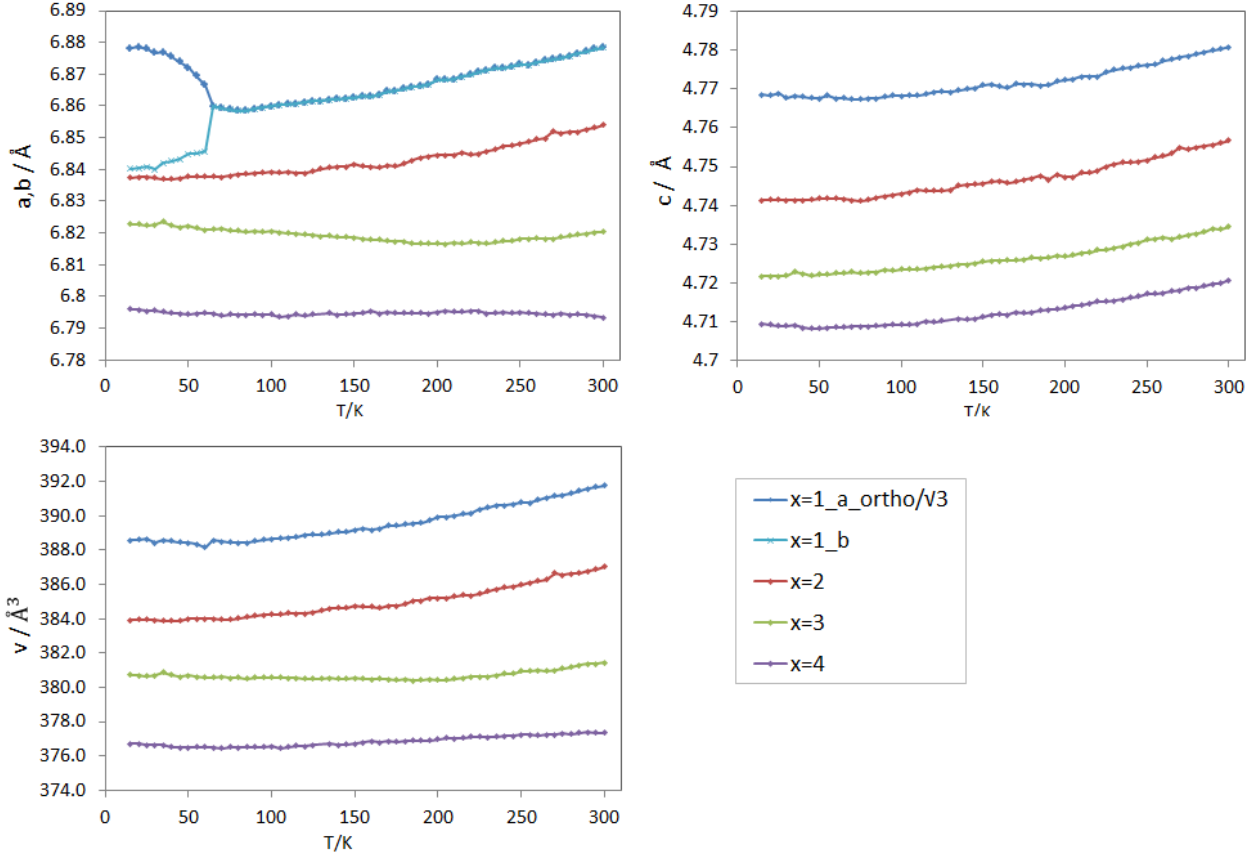
Figure 6.8: Comparison of a (b) - and c- lattice parameter and unit cell volumes for the four individual compounds $Mn_{5-x}Fe_xSi_3$ with x=1, 2, 3, 4. (For Mn_4FeSi_3 in the orthorhombic phase the a-lattice parameter and the unit cell volume have been divided by $\sqrt{3}$). Data for $MnFe_4Si_3$ were taken from [15].

Furthermore, it is interesting to plot the lattice parameters in the four compounds against the unit cell volume, as this allows to identify changes which are not directly a consequence of the volume contraction (or expansion). This is shown in Figure 6.9. The plot shows a linear relationship between the a- and the c-lattice parameter and the unit cell volume for the compound with x=2. For the other three compounds with x=1, 3, 4 the change of the a- and c-lattice parameter as a function of the unit cell volume are far more complex, indicating that the overall change of the unit cell

volume influences the crystal structure in a different way in the a-b-plane and in the c-direction, respectively. To understand this behavior better, more detailed investigations on the temperature dependent behavior of the crystal structures are necessary. In particular, single crystal investigations should be performed to follow the temperature induced changes on the interatomic distances and angles.
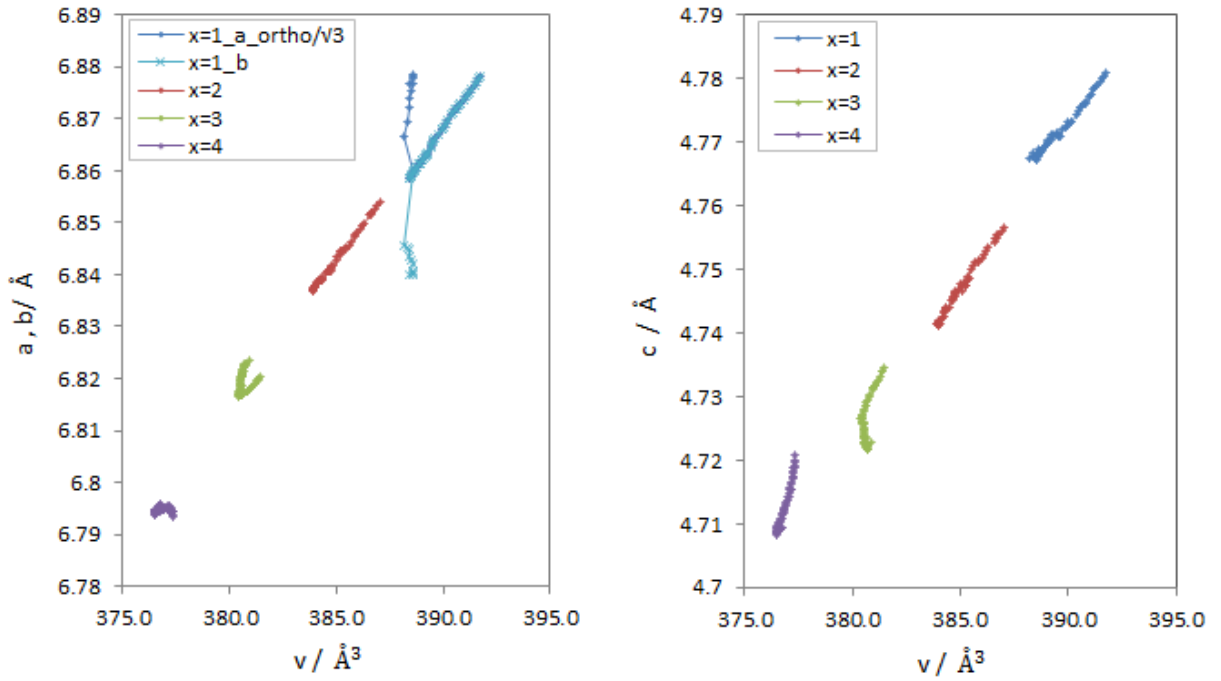
Figure 6.9: Lattice parameters of $Mn_{5-x}Fe_xSi_3$ compounds with x=1, 2, 3, 4 as a function of the unit cell volume. (For Mn_4FeSi_3 in the orthorhombic phase the a-lattice parameter and the unit cell volume have been divided by $\sqrt{3}$). Data for $MnFe_4Si_3$ were taken from [15].

Figure 6.10 shows the c/a ratio against the unit cell volume for the four compounds. As can be seen the c/a ratio drastically varies as a function of the unit cell volume for the compounds with x=3, 4. For the compound with x=2 the variation of the c/a ratio is significantly smaller. For the

compound with x=1 the c/a ratio first decreases with decreasing unit cell volume and then increases till the transition to the orthorhombic phase is reached. The variation of $c/(a_{ortho}/\sqrt{3})$ and c/b in the orthorhombic phase is large and comparable to the variation observed for the compounds with x=3, 4.
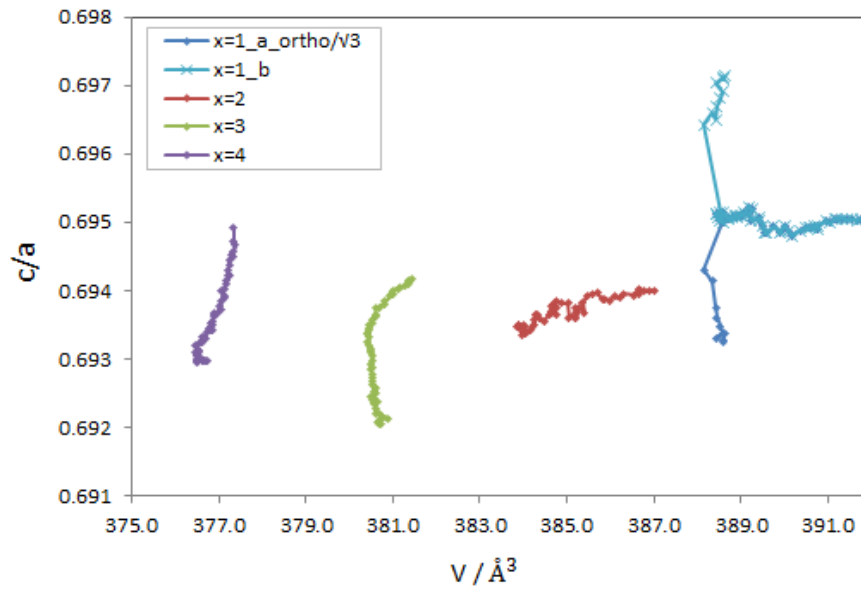
Figure 6.10: The c/a ratio for $Mn_{5-x}Fe_xSi_3$ compounds with x=1, 2, 3, 4 as a function of the unit cell volume. The $c/(a_{ortho}/\sqrt{3})$ and c/b ratio for the orthorhombic phase of Mn_4FeSi_3 are also included.

Chapter 7

Conclusions and outlook

The thermal behavior of the lattice parameter and unit cell volumes of the newly synthesized compounds Mn_4FeSi_3, $Mn_3Fe_2Si_3$ and $Mn_2Fe_3Si_3$ have been studied with X-ray powder diffraction in the temperature range. In contrast to previous study [2], the investigated temperature range was extended to $300\,K$ to $15\,K$ with steps one of $5\,K$.

For the compound Mn_4FeSi_3 a new structural phase transition between $65\,K$ and $60\,K$ was observed in which the symmetry changes from $P6_3/mcm$ to $Cmcm$. The compound $Mn_3Fe_2Si_3$ shows normal thermal expansion over the whole temperature range. The compound with x=3 shows a negative thermal expansion of the a lattice parameter and a continuous decrease of the c-lattice parameter as a function of decreasing temperature and thus behaves similar to $MnFe_4Si_3$ which has been studied earlier [15]. The change in the a- and c-lattice parameter cannot be understood as a function of the unit cell volume for the compounds with x=1, 3, 4. A linear relationship between the change in the a- and c-lattice parameter and the unit cell volume has been only observed for the compound $Mn_3Fe_2Si_3$ (x=2).

In general, most of the magnetic transitions are clearly visible in the lattice parameter and changes in the behavior of the lattice parameter around the magnetic ordering temperatures are significant, indicating a coupling between spin and lattice degrees of freedom in these magnetocaloric compounds.

Several small anomalies are observed in the temperature dependence of the lattice parameter and unit cell volumes. For example, in compound $Mn_3Fe_2Si_3$ (x=2), the anomaly at about $270\,K$ needs further investigation and also the anomaly at $35\,K$ in $Mn_2Fe_3Si_3$ (x=3) should be further studied.

In order to understand the complex behavior of the lattice parameter as a function of the unit cell volume better, single crystal investigations as a function of temperature are warranted to relate the observed variations to changes in individual interatomic distances and angles.

Bibliography

[1] Konstantin P.Skokov James D.Moore J.Liu, T.Gottschall and Oliver Gutfleisch. Giant magnetocaloric effect driven by structural transitions. *Nature Material*, 11(620-626), 2012.

[2] B.Gajić H.Bińczycka, Ž.Dimitrijević and A.szytula. Atomic and magnetic structure of $Mn_{5-x}Fe_xSi_3$. *physica status solidi (a)*, 19(K13-K17), 1973.

[3] O.Tegus E.Brück J.C.P.Klaasse F.R. de Boer Songlin, Dagula and K.H.J.Buschow. Magnetic phase transition and magnetocaloric effect in $Mn_{5-x}Fe_xSi_3$. *Journal of Alloys and Compounds*, 334(249-252), 2002.

[4] Duroy H. Le Bail, A. and J. L. Fourquet. Ab-initio structure determination of $LiSbWO_6$ by X-Ray powder diffraction. *Materials Research Bulletin*, 23(447-452), 1988.

[5] L.Palatinus V.Petricek and M.Dusek. Jana2006 - the crystallographic computing system. Technical report, Institute of Physics, Academy of Science of the Czech Republic, Praha, 2006.

[6] B. Ingale V. Franco, J. S. Blazquez and A. Conde. The magnetocaloric

effect and magnetic refrigeration near room temperature: Materials and models. *Annual Review of Materials Research*, 42(305-342), 2012.

[7] Zbigniew Dauter and Mariusz Jaskolski. How to read (and understand) volume a of international tables for crystallography: an introduction for nonspecialists. *Journal of Applied Crystallography*, 43(1150-1171), 2010.

[8] http://www.ammrf.org.au.

[9] http://www.globalsino.com.

[10] http://www.pd.chem.ucl.ac.uk.

[11] S. Merlin A. Jouan, JP. Moncouyoux and P. Roux. *Multiple Applications of Cold Crucible Melting*. Waste Management' 96, Tucson, 1996.

[12] M.Beyss and H.Gier. Poster, Schmelzverfahren für die Herstellung von Reinstmaterialien. Forschungszentrum Jülich GmbH, Forschungszentrum Jülich GmbH.

[13] http://www.xhuber.de.

[14] G. Bladinozzi and J.F. Berar. *Journal of Applied Crystallography*, 2010.

[15] Paul Hering. *Studium des Magnetokalorischen Effekts in MnFe$_4$Si$_3$*. PhD thesis, Forschungszentrum Jülich GmbH; JCNS-2, 2014.